*Int. J. Heat Mass Transfer.* Vol. 28, No. 9, pp. 1679–1687, 1985
Printed in Great Britain

0017-9310/85 $3.00 + 0.00


# Conjugate heat transfer in a channel with staggered ribs

B. W. WEBB and S. RAMADHYANI
School of Mechanical Engineering, Purdue University,
West Lafayette, IN 47907, U.S.A.

(*Received* 8 *October* 1984 *and in final form* 8 *February* 1985)

**Abstract**—Fluid flow and heat transfer characteristics were analyzed for a constant property fluid flowing laminarly through a parallel plate channel with staggered, transverse ribs and a constant heat flux along both walls. After a finite entry length the flow becomes periodically fully developed. Computations were carried out in the fully-developed regime for different Reynolds numbers, Prandtl numbers, and geometric arrangements. It is found that significant heat transfer augmentation is obtained for high Prandtl number fluids such as water or fluorocarbons. In addition, conduction in the channel walls is found to play a highly beneficial role in enhancing heat transfer.

## 1. INTRODUCTION

THE PROBLEM of convective heat transfer in small channels is of considerable technological interest. Compact heat exchangers and electronic equipment packages represent industrial situations in which channel-flow heat transfer is encountered. The flow in these channels is often laminar due to the small dimensions and low velocities employed, and the heat transfer coefficients are characteristically low. Consequently, a number of ideas have been proposed for heat transfer enhancement in these situations [1]. Fins protruding into the convective flow field form the basis for most of the suggested augmentation techniques. The fins provide more surface area for heat transfer and enhance the mixing in the flow.

One scheme proposed for augmenting heat transfer in parallel plate channels involves mounting a staggered array of transverse ribs as shown in Fig. 1. The ribs cause the flow to deflect and impinge on the opposite wall and its ribs, resulting in a possibly higher heat transfer coefficient than that obtained in the corresponding smooth channel. Three effects are expected in such a flow: (1) the periodic interruption of the thermal boundary layer; (2) the fin effect due to the ribs protruding into the flow; and (3) higher streamwise pressure drops associated with the flow-obstructing ribs. Obviously, the flow and heat transfer will be highly sensitive to the geometric arrangement used. The purpose of this paper is to present results of a numerical study on the hydrodynamic and thermal characteristics of the suggested parallel plate channel with staggered fins on the side walls.

Related work has shown that transverse ribs in the flow field can have either a positive or a negative effect on the heat transfer in the channel. A numerical study of heat transfer in circumferentially finned tubes [2] has shown a decrease in the overall Nusselt number for low Prandtl number fluids, since the ribs cause the main flow to detach entirely from the tube wall. An experimental study of high Prandtl number laminar flow in a circular annulus with circumferential ribs on the inner tube [3] showed heat transfer enhancement as high as eight times that found in the corresponding smooth annulus. This was achieved, however, at the expense of a dramatically higher pressure drop. An investigation of sublimation in a corrugated wall channel [4] revealed only marginal heat/mass transfer enhancement for laminar flow in the naphthalene–air system, for which the Schmidt number was 2.5.

Figure 2 shows schematically the geometric arrangement for this investigation. A series of ribs of

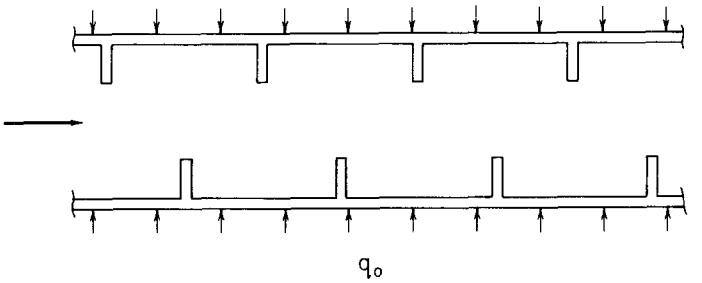


FIG. 1. Schematic of staggered fin array.

## NOMENCLATURE

| | |
|---|---|
| $B$ | channel wall thickness |
| $C_p$ | constant pressure specific heat of fluid |
| $D$ | height of channel, Fig. 2 |
| $D_H$ | channel hydraulic diameter, equation (13) |
| $f$ | Darcy friction factor, equation (11) |
| $\bar{h}$ | module overall heat transfer coefficient based on ribless channel wall area, equation (25) |
| $k$ | thermal conductivity |
| $L$ | rib length, Fig. 2 |
| $\overline{Nu}$ | module overall Nusselt number, equation (24) |
| $p$ | local static pressure |
| $P$ | periodic component of static pressure, equation (1) |
| $Pr$ | fluid Prandtl number, $\mu C_p/k$ |
| $q$ | local heat flux at solid–fluid interface |
| $q_0$ | imposed uniform heat flux at channel exterior |
| $Q_{rib}$ | heat transfer through rib base |
| $Q_{tot}$ | total heat transfer through wall, $2Sq_0$ |
| $Re$ | flow Reynolds number, equation (10) |
| $S$ | spacing between ribs, Fig. 2 |
| $T$ | local temperature |
| $\hat{T}$ | periodic component of local temperature, equation (15) |
| $u$ | fluid velocity in the $x$-direction |
| $\bar{u}$ | average velocity of fluid through channel, equation (12) |
| $v$ | fluid velocity in the $y$-direction |
| $W$ | channel rib thickness, Fig. 2 |
| $x$ | $x$-coordinate, Fig. 2 |
| $y$ | $y$-coordinate, Fig. 2. |

Greek symbols

| | |
|---|---|
| $\beta$ | overall pressure gradient, equation (1) |
| $\mu$ | fluid dynamic viscosity |
| $\nu$ | fluid kinematic viscosity, $\mu/\rho$ |
| $\rho$ | fluid density |
| $\sigma$ | overall temperature gradient, equations (15)–(17) |
| $\psi$ | dimensionless stream function, equations (27), (28). |

Subscripts

| | |
|---|---|
| b | bulk value |
| c | denotes value at center of eddy |
| f | fluid property |
| 0 | ribless parallel plate value |
| s | solid property |
| surf | solid surface value. |

length $L$ and thickness $W$ are spaced equally, a distance $S$ apart, along the length of the channel. Uniform heat flux $q_0$ is applied externally to the side walls of thickness $B$, which are thermally conducting. The side walls redistribute the applied external heat flux by permitting energy to flow to regions of high heat transfer coefficient. The ribs provide partial blockage of the channel of width $D$. The blockage effectively increases the flow velocity and causes the flow to deflect and impinge against the opposite wall and rib. Recirculation zones form as the main flow separates from the rib tips.

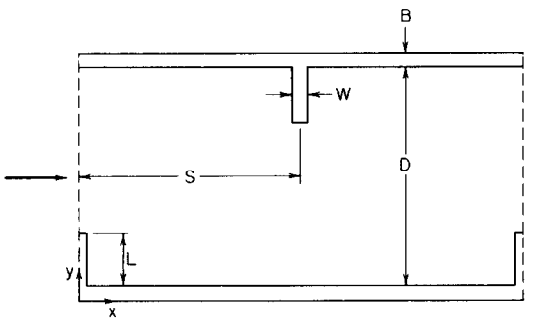


FIG. 2. Computational domain and geometrical parameters.

During the course of the present work a concurrent study [5] came to the attention of the authors treating the problem of heat transfer in ribbed channels with uniform wall temperature boundary conditions. However, neither that study nor any other previous investigation has examined the influence of conjugate heat transfer in the walls. As shown in this study, wall conduction has a pronounced effect on the extent of heat transfer augmentation. The uniform heat flux boundary condition employed in this study is of practical interest to the electronic cooling industry.

Numerical solutions of the problem have been obtained by a finite-difference method under the assumptions that the flow is steady and laminar with constant properties. In separated flows of this kind, there is a possibility of timewise periodicity owing to vortex shedding in the wake of each rib. A recent flow visualization study in a staggered rib channel [6] revealed the onset of vortex shedding at a Reynolds number of 1670. However, the rib heights investigated in that study were substantially greater than in the present work. No experimental results have been found that would demarcate the Reynolds number corresponding to the onset of vortex shedding for the geometric parameters studied here. Since the numerical

treatment of the timewise periodic regime is impractical from the point of view of computational economy, steady-state solutions to the governing differential equations have been obtained in this study.

The results furnished in this paper include stream function contours that illustrate the qualitative features of the flow field. Also included are quantitative information on the variations of the overall Nusselt number and friction factor with the relevant dimensionless parameters of the problem and detailed information on the role played by the ribs in augmenting heat transfer. The numerical findings presented in this paper are qualitatively corroborated by the experimental results of [3, 4, 6].

## 2. ANALYSIS

The flow and heat transfer are assumed to be two-dimensional and laminar with constant properties. Since the geometry consists of a series of identical geometrical modules and the dependence of fluid properties on temperature is ignored, the flow far downstream of the channel entrance is expected to attain a periodic fully-developed character. In this regime, the velocity field is expected to repeat itself from module to module. The concept of fully-developed periodicity and a solution scheme were first presented in [7]. The repetitive flow field makes it possible to calculate the flow and heat transfer for one typical module located far downstream of the entrance as shown in Fig. 2. The calculation for such a single module yields Nusselt number and friction factor data for the particular geometry studied. These data can then be compared with the smooth channel values.

*Flow field*

As explained in [7], the pressure $p$ in a periodically fully-developed flow can be decomposed into two terms

$$p(x, y) = -\beta x + P(x, y). \tag{1}$$

The $\beta x$ term accounts for the global pressure drop, and the quantity $P(x, y)$ is the periodic perturbation about the global pressure drop such that

$$P(x, y) = P(x + 2S, y). \tag{2}$$

The flow is governed by the continuity and momentum equations:

$$\frac{\partial u}{\partial x} + \frac{\partial v}{\partial y} = 0 \tag{3}$$

$$\rho\left(u\frac{\partial u}{\partial x} + v\frac{\partial u}{\partial y}\right) = \beta - \frac{\partial P}{\partial x} + \mu\left(\frac{\partial^2 u}{\partial x^2} + \frac{\partial^2 u}{\partial y^2}\right) \tag{4}$$

$$\rho\left(u\frac{\partial v}{\partial x} + v\frac{\partial v}{\partial y}\right) = -\frac{\partial P}{\partial y} + \mu\left(\frac{\partial^2 v}{\partial x^2} + \frac{\partial^2 v}{\partial y^2}\right). \tag{5}$$

The periodic nature of the flow and the no-slip conditions at the solid surfaces lead to the hydrodynamic boundary conditions

$$\text{top and bottom wall and fin surfaces} \begin{cases} u = 0 & (6) \\ v = 0 & (7) \end{cases}$$

$$\text{left and right boundaries} \begin{cases} u(0, y) = u(2S, y) & (8) \\ v(0, y) = v(2S, y). & (9) \end{cases}$$

The boundary conditions at the left and right boundaries reflect only the periodicity of the flow while making no specification of the inlet flow velocities. Consequently, the flow rate cannot be directly prescribed as an input to the solution scheme. The specification of flow rate is implicit in the prescription of the global pressure gradient parameter, $\beta$, since $\beta$ must be given in order to solve equations (3)–(5). For a given value of $\beta$ there is a corresponding unique value of the flow rate in the channel. The value of $\beta$ can therefore be adjusted iteratively in the solution scheme to produce a desired value of flow rate, or Reynolds number. The hydrodynamic problem can therefore be seen to be governed by the flow Reynolds number and the geometric parameters $S/D$, $L/D$, and $W/D$. In the present study, the rib thickness ratio $W/D$ was fixed at 0.05. The Reynolds number and friction factor are defined as

$$Re = \frac{\rho \bar{u} D_H}{\mu} \tag{10}$$

and

$$f = \frac{\beta D_H}{\frac{1}{2}\rho \bar{u}^2} \tag{11}$$

where

$$\bar{u} = \frac{1}{D}\int_0^D u\,dy \tag{12}$$

and the channel hydraulic diameter is given by

$$D_H = 2D. \tag{13}$$

It may be noted that the definition for the hydraulic diameter $D_H$ does not account for the increased flow obstruction caused by the presence of the ribs. This permits a direct comparison of the values of $f$ with those for the smooth channel at the same value of $Re$.

*Temperature field*

The governing equation for the temperature field is

$$\rho C_p\left(u\frac{\partial T}{\partial x} + v\frac{\partial T}{\partial y}\right) = k\left(\frac{\partial^2 T}{\partial x^2} + \frac{\partial^2 T}{\partial y^2}\right). \tag{14}$$

The thermal boundary condition studied here is that of uniform heat flux, $q_0$, applied externally to both top and bottom walls. This condition leads to a thermally fully-developed regime which is periodic in nature. Similar to the pressure field, the temperature field is comprised of two components

$$T(x, y) = \sigma x + \hat{T}(x, y). \tag{15}$$

The term $\sigma$ accounts for the global temperature rise

along the channel due to the applied heat flux

$$\sigma = \frac{T(x+2S, y) - T(x, y)}{2S} \tag{16}$$

from which it may be shown that

$$\sigma = \frac{2q_0}{\rho \bar{u} C_p D}. \tag{17}$$

Furthermore, the perturbation $\hat{T}(x, y)$ is repeated from module to module such that

$$\hat{T}(x, y) = \hat{T}(x+2S, y). \tag{18}$$

Introduction of equation (15) in the energy equation (14) yields

$$\rho C_p\left(u\frac{\partial \hat{T}}{\partial x} + v\frac{\partial \hat{T}}{\partial y}\right) = k\left(\frac{\partial^2 \hat{T}}{\partial x^2} + \frac{\partial^2 \hat{T}}{\partial y^2}\right) - \rho C_p \sigma u. \tag{19}$$

The boundary conditions for the periodic temperature fluctuation are:

$$\text{top and bottom walls} \quad \pm k_s \frac{\partial \hat{T}}{\partial y} = q_0 \tag{20}$$

(where the appropriate sign is used for each wall);

$$\text{left and right sides} \quad \hat{T}(0, y) = \hat{T}(2S, y). \tag{21}$$

Additionally, the points of solid–fluid contact must maintain continuity of both heat flux and temperature such that

$$k_s \frac{\partial \hat{T}_s}{\partial n} = k_f \frac{\partial \hat{T}}{\partial n} \tag{22}$$

and

$$\hat{T}_s = \hat{T} \tag{23}$$

where the partial derivative with respect to $n$ indicates a normal derivative. The thermal problem introduces three more dimensionless parameters which must be specified for the solution, namely $Pr$, $k_s/k_f$ and the dimensionless wall thickness $B/D$. However, in the present study $k_s/k_f$ was fixed at a typical representative value of 200. $B/D$ was assigned a value of either 0 or 0.05, corresponding to thermally inactive or active walls, respectively. Thus, the sole thermal parameter of the problem is the Prandtl number, $Pr$.

The overall Nusselt number, an outcome of the solution for the thermal field, is defined as

$$\overline{Nu} = \frac{\bar{h} D_H}{k_f} \tag{24}$$

where

$$\bar{h} = q/(\hat{T}_{surf} - \hat{T}_b). \tag{25}$$

This definition of Nusselt number, based on the smooth channel heat transfer area, permits a direct comparison between the smooth and ribbed channels. The surface temperature used in (25) is the average over the module, and the bulk temperature is defined so as to properly account for regions of reverse flow

$$\hat{T}_b = \int_0^D |u| \hat{T}\, dy \Big/ \int_0^D |u|\, dy. \tag{26}$$

The above definition of the bulk temperature for recirculating flows was proposed in [7].

*Computational details*

The governing equations were solved numerically by a finite-difference scheme, the details of which can be found in ref. [8]. The SIMPLER algorithm was used for prediction of the flow field. In the solution of the velocity field, the solid wall and rib regions were handled by specifying a very large value of the viscosity in that region, as outlined in ref. [9]. Solution for a given Reynolds number was achieved by iteratively updating the value of the global pressure gradient parameter, $\beta$, until convergence was reached.

All computations were performed on a $26 \times 26$ grid. Nodes were clustered near all solid surfaces in order to effectively resolve the strong gradients present there. Under-relaxation was necessary in the solution of the momentum equations, which typically required 400–500 iterations for convergence. The converged hydrodynamic solution data then served as input to the solution of the energy equation. Initial exploratory solutions on progressively finer grids led to an estimation of the overall accuracy of the integral results of about 5% for the final $26 \times 26$ grid.

The effect of the Reynolds number on flow and heat transfer was studied by varying $Re$ from 340 to 2000 for $S/D = 1.0$ and two values of $L/D$, 0.125 and 0.25. The rib height effect was analyzed by varying $L/D$ from 0.0625 to 0.375 for $Re = 340$ and $S/D = 1.0$. Rib spacing was studied in the range of $S/D$ from 0.5 to 2.0 for $Re = 340$ and $L/D = 0.25$. The influence of the conducting top and bottom walls on the heat transfer was investigated for all of the above cases by obtaining thermal solutions for both $B/D = 0$ and $B/D = 0.05$. The Prandtl number dependence was analyzed by solving the energy equation for $Pr = 0.7$ and $Pr = 7.0$ for all the velocity fields computed.

## RESULTS AND DISCUSSION

*Hydrodynamic solutions*

The effects of $Re$, $S/D$, and $L/D$ on the flow field are shown in Figs. 3–5, respectively. The streamlines depicted in these figures are obtained by joining points of equal stream function. The dimensionless stream function $\psi$ is obtained from the velocity field solutions by means of the pair of equations:

$$\psi_{x,y=0} = \psi_{x=0,y=0} - \frac{1}{v}\int_0^x v\, dx \tag{27}$$

$$\psi_{x,y} = \psi_{x,y=0} + \frac{1}{v}\int_0^y u\, dy \tag{28}$$

$\psi_{x=0,y=0}$ was taken arbitrarily to be zero. It may be seen

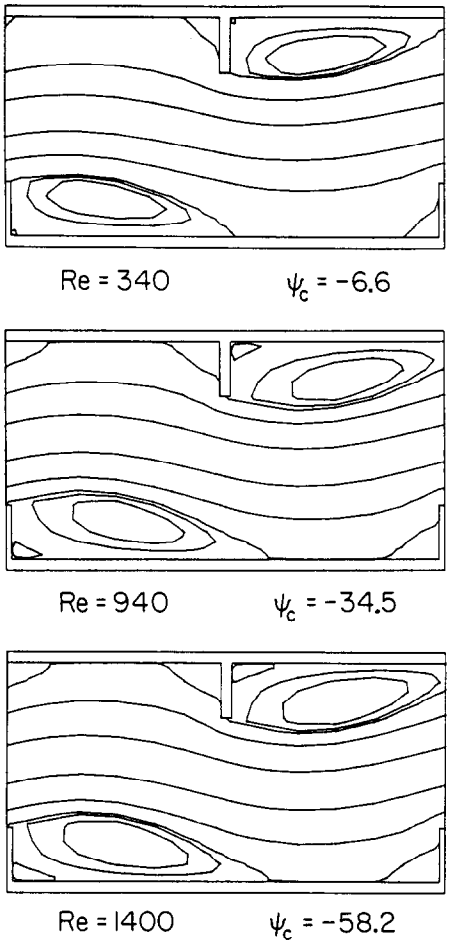


FIG. 3. Streamlines for different Reynolds numbers, $L/D = 0.25$, $S/D = 1.0$.

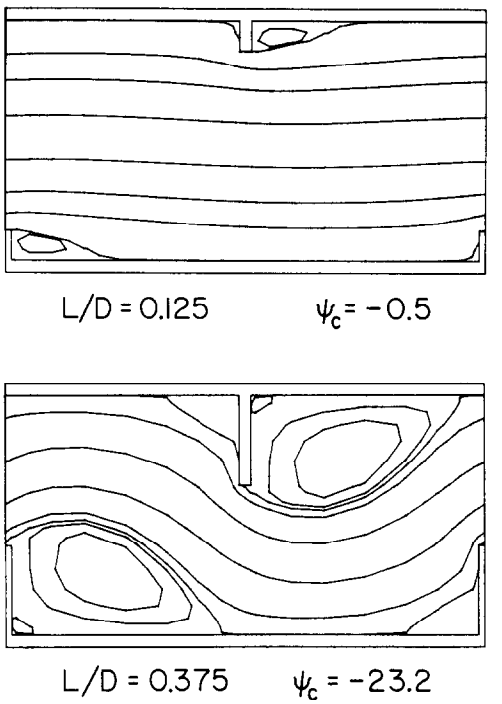


FIG. 5. Streamlines for different rib heights, $S/D = 1.0$, $Re = 340$.

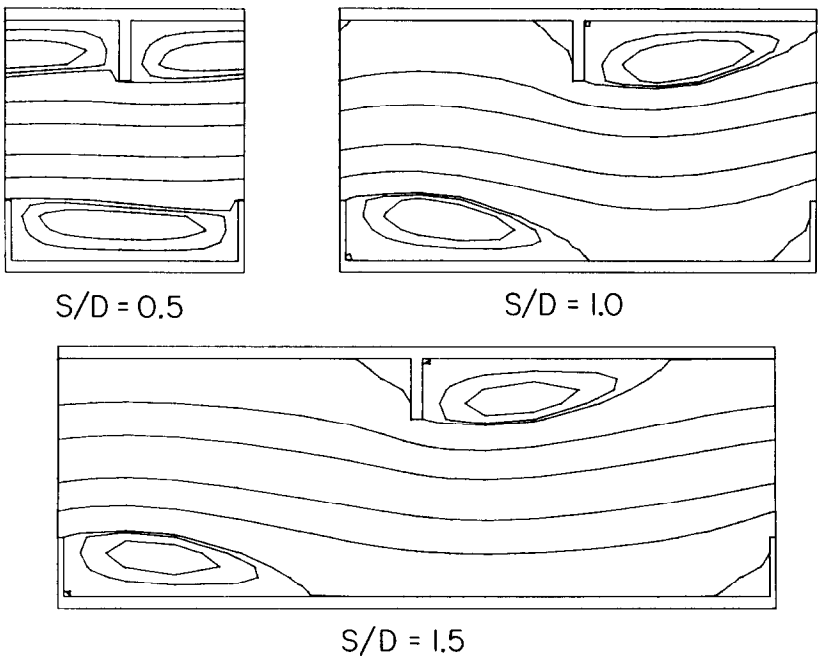


FIG. 4. Streamlines for different rib spacings, $L/D = 0.25$, $Re = 340$.

that the protruding ribs result in radical changes in the flow pattern, the flow being deflected and impinging against the opposite wall. Major recirculation zones are present downstream of the ribs where the flow separates, and smaller eddies may be noted upstream of the ribs.

Figure 3 illustrates the influence of $Re$ on the flow field. The point of reattachment of the flow separating from the fin tip is no longer sensitive to the Reynolds number beyond $Re = 940$, for the geometric configuration shown. In addition, as demonstrated by the relative magnitudes of the stream function at the eddy center, $\psi_c$, the strength of the separated flow increases with $Re$. The size of the eddy on the upstream side of the ribs also increases with increasing $Re$. These observations were also made for the $Re = 2000$ data not shown in the figure. It is interesting to note that the streamlines in the central part of the channel are only slightly deflected by the ribs. Attention is also drawn to the small secondary vortices in the downstream corner of each rib. As will be shown later, the weak recirculating flow in these vortices tends to inhibit heat transfer from the leeward face of each rib.

The effect of rib spacing on the flow field is shown in Fig. 4. As the rib spacing is decreased, the recirculation zone occupies more and more of the exposed wall between the ribs until finally, a full recirculation cell isolates the core flow from the walls. This was not observed in [5] where greater rib heights were analyzed. However, a similar phenomenon was reported in [2] for circumferential ribs in tubes. As will be shown later, the formation of this full recirculation cell has a profound impact on the friction factor and Nusselt number results.

Figure 5 presents the influence of rib height on the flow field. The streamlines are deflected and the flow impinges with greater strength against the opposite wall as the ribs are lengthened. The size and strength of the recirculation zone also increases. For a given Reynolds number, higher velocities are found in the 'core' flow region for the longer ribs. Similar flow patterns were found experimentally in [6].

*Heat transfer and friction factor*

The overall heat transfer and friction factor results are presented in terms of the ratio of the ribbed channel value to the smooth channel value, $\overline{Nu}/Nu_0$ and $fRe/(fRe)_0$, respectively. The values of $Nu_0$ and $(fRe)_0$ are 8.23 and 96, respectively. Values of $\overline{Nu}/Nu_0$ greater than unity indicate desired augmentation of heat transfer while values of $fRe/(fRe)_0$ greater than unity reveal the pressure drop penalty for the obstructing ribs. The plotted symbols indicate actual results of the computations.

Figures 6 and 7 show the variation of overall Nusselt number and friction factor with Reynolds number for $S/D = 1.0$ and $L/D = 0.125$ and 0.25, respectively. Unlike the smooth channel case, the results for the staggered rib channel display a strong Reynolds

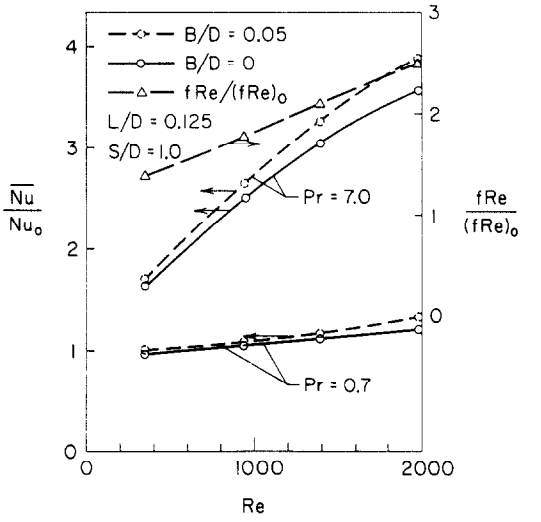


FIG. 6. Variation of friction factor and overall Nusselt number with Reynolds number, $L/D = 0.125$, $S/D = 1.0$.

number and Prandtl number dependence. Both overall Nusselt number and friction factor show an increasing trend with $Re$. That trend is stronger for the longer ribs ($L/D = 0.25$, Fig. 7) as one might expect. The heat transfer results illustrate that the augmentation is substantially higher for higher Prandtl numbers; $\overline{Nu}/Nu_0$ for $Pr = 7.0$ can be as much as 350% greater than the $Pr = 0.7$ data in the high Reynolds number range. The experimental results of [3,4] also substantiate qualitatively this Prandtl number dependence.

Heat transfer augmentation is evidenced in all cases except at low $Re$ for $L/D = 0.125, B/D = 0, Pr = 0.7$. In this case $\overline{Nu}/Nu_0$ actually falls below unity indicating a decrease in heat transfer due to the presence of the ribs. Similar numerical results were found in [2, 5]. It may be

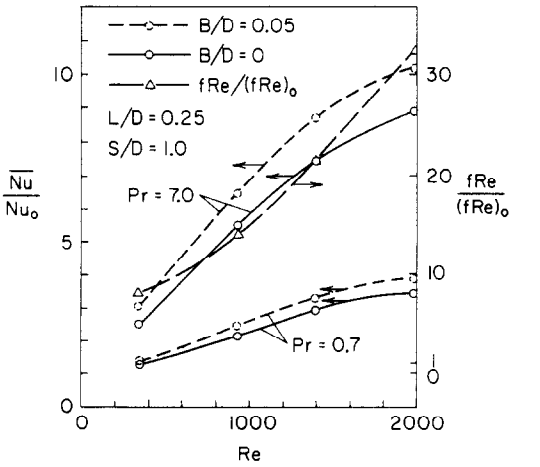


FIG. 7. Variation of friction factor and overall Nusselt number with Reynolds number, $L/D = 0.25$, $S/D = 1.0$.

noted, however, that the presence of the conducting top and bottom walls ($B/D = 0.05$) alleviates this decrease in heat transfer in the low $Re$ range.

The addition of the conducting walls to the analysis reveals a positive heat transfer influence in all cases. The $Nu/Nu_0$ data for the conducting top and bottom wall cases are always 5–25% higher than the corresponding data for the $B/D = 0$ case. This is a result of the lateral redistribution of energy flow possible in ribbed channels with conducting walls. In the case of the nonconducting wall ($B/D = 0$), lateral redistribution of the applied heat flux $q_0$ is not possible. In this case ($B/D = 0$), heat transfer augmentation is effected by two mechanisms: (a) periodic interruption of the thermal boundary layer; and (b) flow impingement on the channel walls downstream of each rib. In the case of the conducting wall ($B/D = 0.05$), the lateral redistribution of energy towards the ribs leads to additional heat transfer augmentation.

It should be noted that despite the increase in overall Nusselt number, there is a dramatic penalty in terms of required pumping power. For $L/D = 0.25$, $Re = 2000$, the overall Nusselt number for $Pr = 7.0$ and $B/D = 0.05$ is approximately 10 times greater than the smooth channel value, while the corresponding frictional pressure drop is over 30 times greater than that for a similar smooth channel. In this case, the increased pressure drop penalty paid for improved heat transfer characteristics in the high Reynolds number range is probably not justified.

The effect of rib length on heat transfer and friction factor characteristics is presented in Fig. 8. The heat transfer is actually decreased for $Pr = 0.7$, and with shorter ribs ($L/D \approx 0.125$). However, there is a substantial augmentation of heat transfer for the higher Prandtl number fluid. In all cases the presence of conducting top and bottom walls has a favorable effect on the heat transfer. The friction factor data show that rib heights of $L/D > 0.25$ probably cannot be justified since a 'knee' in the curve occurs there. For $L/D$ greater than 0.25 the increased pumping power requirement is too costly to justify the increased heat transfer. The results indicate that for fluids of low Prandtl number, such as gases, only marginal heat transfer augmentation may be expected.

Figure 9, which depicts the influence of rib spacing, corroborates the conclusion reached above. It appears that there is very little heat transfer augmentation for low Prandtl number fluids regardless of rib spacing. A maximum overall Nusselt number occurs at a rib spacing of about $S/D = 1.0$ for both Prandtl numbers. Again, the heat transfer for $B/D = 0.05$ is always higher than for the zero wall thickness case, $B/D = 0$. As the rib spacing is decreased the friction factor increases dramatically until it levels off at about $S/D = 0.75$. This is the result of the formation of a full recirculation cell between the ribs, as seen in Fig. 4. The resulting new 'core' flow regime prevents the fluid from washing the wall and rib sides. It is no coincidence that the overall Nusselt number falls dramatically for decreasing $S/D$ after the formation of this full recirculation cell. This same phenomenon was observed in tubes with circumferential ribs [2]. However, no mention of this was made in a related work [5] which investigated staggered ribs in a parallel plate channel; the rib heights principally used in that study were long enough to prevent the formation of a full recirculation cell between the ribs. The data show that for rib spacing $S/D$ between 1.0 and 1.5, the friction factor is relatively low and the Nusselt number still relatively high. Again, the presence of such ribs is probably only justified for higher Prandtl number fluids.

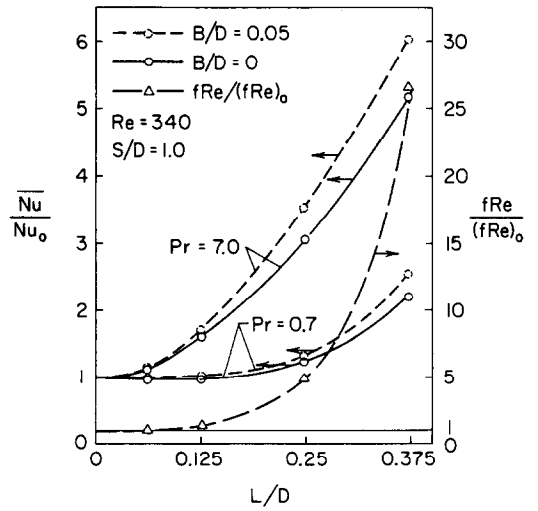


FIG. 8. Variation of friction factor and overall Nusselt number with rib height, $S/D = 1.0$, $Re = 340$.

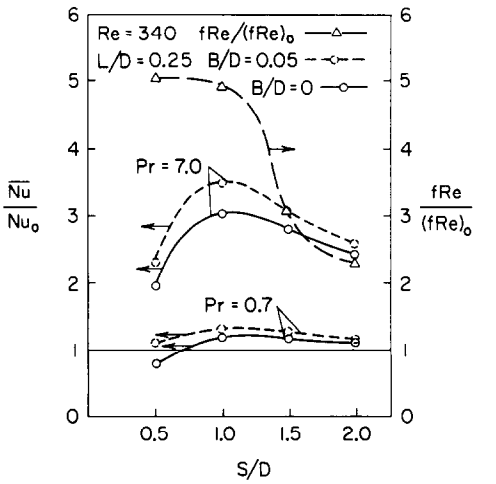


FIG. 9. Variation of friction factor and overall Nusselt number with rib spacing, $L/D = 0.25$, $Re = 340$.

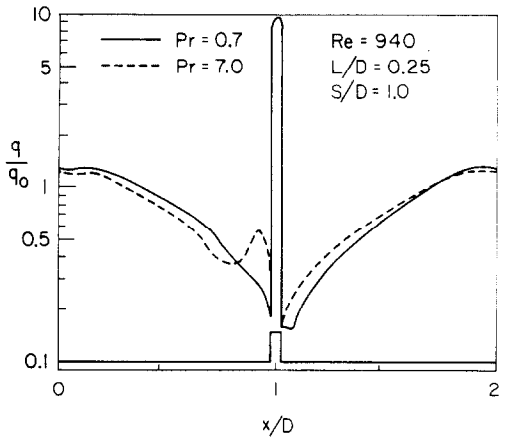


FIG. 10. Local heat flux at solid–fluid interface, $Re = 940$, $L/D = 0.25$, $S/D = 1.0$.

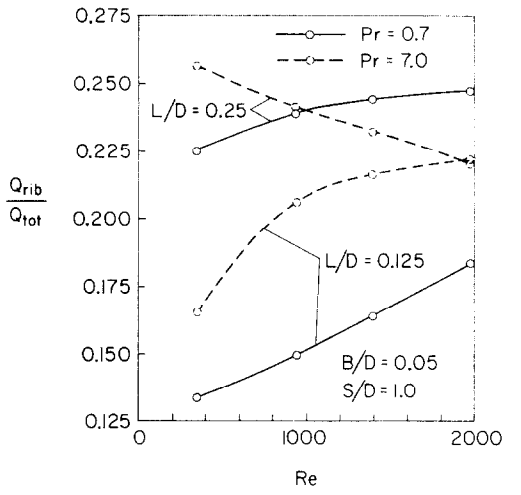


FIG. 12. Variation of rib heat transfer with Reynolds number, $B/D = 0.05$, $S/D = 1.0$.

*Local heat transfer*

Figure 10 shows the local dimensionless heat flux at the solid–fluid interface along the top wall. The value of $q/q_0$ shown at the rib is the heat transfer through its base. The case shown is representative of all cases with $B/D = 0.05$. Of course, for $B/D = 0$, $q/q_0 = 1$. The figure illustrates how the presence of the conducting wall permits the redistribution of energy flow to regions where the heat transfer coefficient is high. In the circulation zones near the base of the rib the flow velocity is relatively low, resulting in a low heat flux there. As shown by the local maximum immediately upstream of the rib, higher Prandtl number fluids produce more effective heat transfer from the wall in the recirculation zone. This higher effectiveness for high Prandtl number fluids is even greater at higher Reynolds numbers (not shown). A large fraction of the energy is re-routed through the wall into the fin where high impingement velocities result in very effective heat transfer. This is evidenced by the 'spike' in $q/q_0$ at the rib, seen for both Prandtl numbers. The conducting wall therefore has a very favorable influence on the heat transfer.

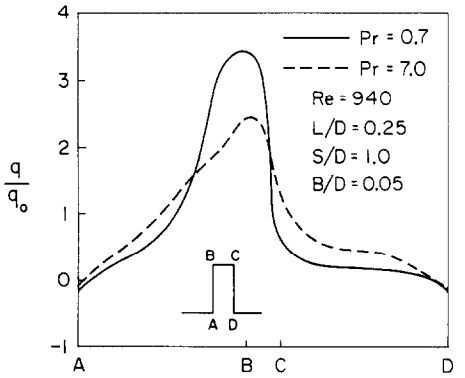


FIG. 11. Local heat flux along rib surface, $Re = 940$, $L/D = 0.25$, $S/D = 1.0$, $B/D = 0.05$.

The local heat flux along the rib surface is shown in Fig. 11. The rib perimeter has been expanded linearly along the abcissa of the figure. Attention is drawn to the fact that $q/q_0$ drops below zero near points A and D. At these locations, where the fluid is nearly stagnant, the direction of energy flow is actually from the fluid to the solid rib. The highest heat transfer occurs on the upstream side of the rib and at the rib tip where the influence of the high impingement velocities is most pronounced. The local heat flux drops rapidly on the downstream side of the rib where recirculation velocities are low. The shape of the $Pr = 0.7$ curve shows that the maximum heat flux occurs near the rib tip while the region near the base is relatively inactive. In comparison, for $Pr = 7.0$, the $q/q_0$ profile is more nearly uniform along the periphery of the rib.

The fraction of the total wall heat transfer that passes through the base of the rib is shown as a function of Reynolds number in Fig. 12. The thermal effectiveness of the rib is measured by the fact that although it occupies only 2.5% of the area, 15–25% of the total heat transfer takes place there. The rib heat transfer increases with Reynolds number for all cases except the $L/D = 0.25$, $Pr = 7.0$ case. This decreasing rib effectiveness with increasing $Re$ may be explained as follows: in the case of $L/D = 0.25$ large recirculation zones exist both upstream and downstream of the fin. For the higher Prandtl number fluid, heat transfer from the wall to the recirculating fluid increases strongly with $Re$. Thus, the rib is partially depleted of its supply of energy and its effectiveness diminishes.

## CONCLUSIONS

Numerical predictions were made for flow and heat transfer in a parallel plate channel with staggered ribs. The influence of conjugate heat transfer in the top and bottom walls was also investigated. The protruding ribs result in the formation of separated zones in the flow

field, yielding substantially higher friction factors. The presence of conducting channel walls yields significantly higher overall Nusselt numbers due to the lateral redistribution of energy flow. The geometrical configuration of approx. $L/D = 0.25$ and $S/D = 1.5$ yields a combination of increased overall Nusselt number and comparatively low resulting friction factor. However, the augmentation of heat transfer under these conditions is probably only justifiable for high Prandtl number fluids such as water or fluorocarbons. The increase in heat transfer for gases ($Pr = 0.7$) is not substantial enough to offset the added friction factor penalty.

*Acknowledgements*—One of the authors (B. W. Webb) acknowledges financial support of his studies by an Eastman Kodak Company Graduate Fellowship. Computing facilities were made available by the Purdue University Computer Center.

## REFERENCES

1. A. E. Bergles and S. D. Joshi, Augmentation techniques for low Reynolds number in-tube flow. In *Low Reynolds Number Heat Exchangers* (edited by S. Kakac, R. K. Shah and A. E. Bergles), pp. 695–720. Hemisphere, Washington (1981).
2. G. J. Rowley and S. V. Patankar, Analysis of laminar flow and heat transfer in tubes with internal circumferential fins, *Int. J. Heat Mass Transfer* **27**, 553–560 (1984).
3. G. E. Geiger and S. K. Mandal, Heat transfer and friction factors of high Prandtl number laminar flow through an annulus with circumferential fins. *Proc. 6th Int. Heat Transfer Conference*, Toronto, Vol. 2, pp. 607–611 (1978).
4. L. Goldstein and E. M. Sparrow, Heat/mass transfer characteristics for flow in a corrugated wall channel, *Trans. Am. Soc. mech. Engrs, J. Heat Transfer* **99**, 187–195 (1977).
5. K. M. Kelkar and S. V. Patankar, Numerical prediction of flow and heat transfer in a parallel plate channel with staggered fins, paper no. 84-HT-70, ASME/AIChE National Heat Transfer Conference, Niagara Falls, New York (1984).
6. C. Berner, F. Durst and D. M. McEligot, Flow around baffles, *Trans. Am. Soc. mech. Engrs, J. Heat Transfer* **106**, 743–749 (1984).
7. S. V. Patankar, C. H. Liu and E. M. Sparrow, Fully developed flow and heat transfer in ducts having streamwise-periodic variations of cross-sectional area, *Trans. Am. Soc. mech. Engrs, J. Heat Transfer* **99**, 180–186 (1977).
8. S. V. Patankar, *Numerical Heat Transfer and Fluid Flow*. McGraw-Hill, New York (1980).
9. S. V. Patankar, A numerical method for conduction in composite materials, flow in irregular geometries, and conjugate heat transfer. *Proc. 6th Int. Heat Transfer Conference*, Toronto, Vol. 3, pp. 297–302 (1978).

## TRANSFERT THERMIQUE CONJUGUE DANS UN CANAL AVEC DES ENTRETOISES ETAGEES

**Résumé**—Des caractéristiques d'écoulement et de transfert thermiques sont analysées pour un fluide à propriétés constantes qui s'écoule laminairement à travers un canal entre plans parallèles avec des entretoises transverses et étagées et un flux uniforme le long des parois. Après une longueur d'entrée finie, l'écoulement devient périodiquement pleinement développé. Des calculs sont menés dans le régime pleinement développé pour différents nombres de Reynolds, de Prandtl et différents arrangements géométriques. On trouve qu'une augmentation sensible du transfert thermique est obtenue pour des fluides à nombres de Prandtl élevés tels que l'eau ou les fluorocarbures. De plus, la conduction dans les parois joue un rôle fortement bénéfique dans l'accroissement du transfert thermique.

## WÄRMEÜBERGANG IN EINEM KANAL MIT VERSETZT ANGEORDNETEN RIPPEN

**Zusammenfassung**—Für ein Fluid mit konstanten Stoffeigenschaften wurde das Strömungs- und Wärmeübergangsverhalten bei laminarer Strömung durch einen Kanal aus parallelen Platten mit versetzt angeordneten Querrippen und einem konstanten Wärmestrom an beiden Kanalwänden untersucht. Nach einer begrenzten Einlauflänge wurde die Strömung periodisch voll ausgebildet. Bei voll ausgebildten Strömungsverhältnissen wurden Berechnungen für unterschiedliche Reynolds-Zahlen, Prandtl-Zahlen und geometrische Anordnungen durchgeführt. Es stellte sich heraus, daß man mit Fluiden von großer Prandtl-Zahl, wie Wasser oder Fluorkohlenwasserstoff, bedeutende Verbesserungen des Wärmeübergangs erreichen kann. Desweiteren konnte gezeigt werden, daß Wärmeleitung in den Kanalwänden stark zur Verbesserung des Wärmeübergangs beiträgt.

## СОПРЯЖЕННЫЙ ТЕПЛОПЕРЕНОС В КАНАЛЕ С РЕБРАМИ, РАСПОЛОЖЕННЫМИ В ШАХМАТНОМ ПОРЯДКЕ

**Аннотация**—Характеристики течения жидкости и теплообмена проанализированы для жидкости с постоянными свойствами, движущейся в ламинарном режиме через плоско-параллельный канал с расположенными в шахматном порядке поперек течения ребрами и постоянным тепловым потоком вдоль обеих стенок. После прохождения входного участка конечной длины течение становится периодически полностью развитым. Проведены расчеты в полностью развитом режиме для различных чисел Рейнольдса, Прандтля и разных геометрий. Найдено, что существенная интенсификация теплообмена получена для жидкостей с большим числом Прандтля, таких как вода или фтороуглероды. Также обнаружено, что теплопроводность стенок канала играет важную роль в интенсификации теплообмена.